electronics

MDPI

Article

A Fault Diagnosis Method for Turnout Switch Machines Based on Sound Signals

Yong Li [1,*], Xinyi Tao [2] and Yongkui Sun [2]

[1] Public Security Department, Fujian Police College, Fuzhou 350007, China
[2] School of Automation and Intelligence, Beijing Jiaotong University, Beijing 100044, China; sunyk@bjtu.edu.cn (Y.S.)
* Correspondence: yl112@fjpsc.edu.cn

Abstract: The turnout switch machine, a vital outdoor component of railway signaling, controls train steering amidst complex operations and high frequencies. Its malfunction significantly disrupts train operations, potentially causing derailments. This paper proposes a sound-based fault diagnosis method, termed ERS (a method combining EMD, ReliefF, and SVM), for effective monitoring and detection of turnout switch machines. The method employs Eigenmode Decomposition (EMD) to smooth the sound signal, reduce noise, and extract key statistical parameters of both the time and frequency domains. To address redundant information in high-dimensional features, the ReliefF algorithm is utilized for feature selection, dimension reduction, and fault classification based on weighted parameters. Subsequently, the selected feature parameters are used to train the Support Vector Machine (SVM). A comparison with results obtained without ReliefF feature selection demonstrates the necessity of this step. The results show that the fault diagnosis accuracy reaches 98% in the positioning work mode and 95.67% in the reversing work mode, verifying the method's effectiveness and feasibility.

Keywords: turnout switch machine; fault diagnosis; EMD-ReliefF-SVM; feature selection

check for updates

Citation: Li, Y.; Tao, X.; Sun, Y. A Fault Diagnosis Method for Turnout Switch Machines Based on Sound Signals. *Electronics* **2024**, *13*, 4839. https://doi.org/10.3390/electronics13234839

Received: 31 October 2024
Revised: 26 November 2024
Accepted: 4 December 2024
Published: 7 December 2024

Copyright: © 2024 by the authors. Licensee MDPI, Basel, Switzerland. This article is an open access article distributed under the terms and conditions of the Creative Commons Attribution (CC BY) license (https://creativecommons.org/licenses/by/4.0/).

1. Introduction

In recent years, high-speed railways have achieved rapid development in the world. The problem of fault diagnosis of rail transportation systems has increasingly attracted extensive attention from society. Specifically, the turnout switch machine is an important piece of equipment to ensure the efficient and safe operation of the railway, which is directly related to whether the train can run safely. Statistics show that the number of faults always accounts for the first place in the railway signaling system (about 40%). Therefore, it is of great significance to develop an efficient fault diagnosis method for turnouts.

Recent years, many scholars have performed many studies on fault diagnosis of switch machines. The current landscape of fault diagnosis methods for turnout switch machines can be summarized as the threshold method [1,2], the expert system method [3], and the signal processing method [4–10].

In terms of the threshold methods, they rely heavily on empirical data and are susceptible to the vagaries of subjective interpretation. The threshold method detects faults by setting empirical thresholds for the dynamic time of the turnout motor current, and one of the commonly used ways is dynamic time wrapping [1,2]. The key step of the method is the setting of thresholds. For example, Gao et al. proposed a threshold-based method using FastDTW under big data monitoring [1]. However, it is prone to subjective judgment since the thresholds are set based on experience. In addition, due to the influence of various external conditions and different conditions of the equipment itself on each fault, there is significant randomness. This results in relatively large errors and low accuracy. Additionally, the threshold method can only determine the occurrence of a fault but cannot identify the cause of the fault.

For the expert system, it gains a comprehensive understanding of faults through the accumulation of a sufficient quantity of experience. It can identify both the occurrence of faults and their underlying causes. For example, Reetz et al. presented an expert-system-based fault diagnosis method for railway switch machines by combining multiple sources of information [3]. However, it is heavily influenced by factors of human control, lacks objectivity, and is prone to affecting judgment results, even though it has high accuracy and strong flexibility.

In light of these above challenges, the field has witnessed a surge in innovative solutions that leverage advancements in signal processing [4–6]. For example, Lao et al. proposed a fault diagnosis for a switch machine based on multiscale permutation entropy, adaptive feature selection, and improved LightGBM to distinguish samples with similar categories for higher diagnostic accuracy [7]. Wang et al. proposed a fault diagnosis method based on maximal relevancy, minimal redundancy, and a cost-sensitive Extreme Learning Machine, which had better stability and generalization than traditional methods [8]. Abbasnejad et al. proposed a fault prediction method for rotational speed, based on Autoregressive Integrated Moving Average (ARIMA) and Autoregressive Kalman methods, which utilize wavelet transform to extract fault trends in ball screws and gears, enabling fault detection and diagnosis [9]. Shi et al. proposed a method based on auto-associative residuals for assessing the health status and diagnosing faults in switch machines and achieved the advantage of requiring less expert knowledge for model development [10]. Accordingly, the signal processing method can effectively address issues present in traditional fault diagnosis methods, such as the inability to identify the causes of faults, the need for a large amount of expert experience, and the significant influence of the subject.

In general, the motor current and voltage signals of the switch machine are the acquired data for processing. However, the integration of vibration signal analysis also has shown promise, offering a non-invasive approach to diagnosing faults by interpreting the mechanical signatures embedded within the vibration data. Since the vibration signals of the switch machine contain rich mechanical information, the fault information is complex and diverse, prone to interference, and easily affected by noise. Therefore, misjudgment, missed judgment, and misdiagnosis often occur during monitoring. To address these issues, a method based on sound analysis utilizes Mel-frequency cepstrum coefficients (MFCCs) and SVM to effectively detect faults in rail transit signals [11]. The method can effectively extract characteristic information from rail transit signals and employ SVM for classification and recognition, thereby achieving effective detection and diagnosis of rail transit signals. A fault diagnosis method for railway point machines using VMD and multiscale fluctuation-based dispersion entropy was proposed based on vibration signals [4]. Apart from traditional machine learning methods, big data technology [12–15] and data fusion [16,17] are also important, but obtaining a large amount of comprehensive data for data processing is difficult and expensive. Furthermore, the existing methods are easily influenced by human factors, with conditions that are not objective, which reduces accuracy.

Therefore, to achieve better performance for the fault diagnosis of switch machines, considering the advantages of easy collection and contactlessness of sound signals, this paper proposes a sound-signal-based fault diagnosis method, namely ERS (a method combining EMD, ReliefF, and SVM), for the turnout switch machine. First, employed as a favored technique for handling signals that are both non-stationary and nonlinear, EMD is applied to the preliminary processing of the sound signals [18–24]. The initial 15 intrinsic mode functions' statistical characteristics in both time and frequency domains are utilized to form the feature vector. To quickly reduce the insufficient features, the ReliefF algorithm is used to realize feature dimensionality reduction [25,26]. Finally, SVM is selected for fault diagnosis due to its applicability to small samples.

This paper is organized as follows. Section 2 introduces the fault diagnosis method. Section 3 presents experiment results and analysis. Section 4 draws the conclusion.

2. Methodology

Considering the advantages of EMD, our work utilized EMD to preprocess sound signals to extract both time domain and frequency domain information. Then, the ReliefF algorithm was utilized to select the features. Finally, the types of faults in the turnout switch machine were determined by classifying the combined characteristics using SVM. Its execution process is shown in Figure 1.

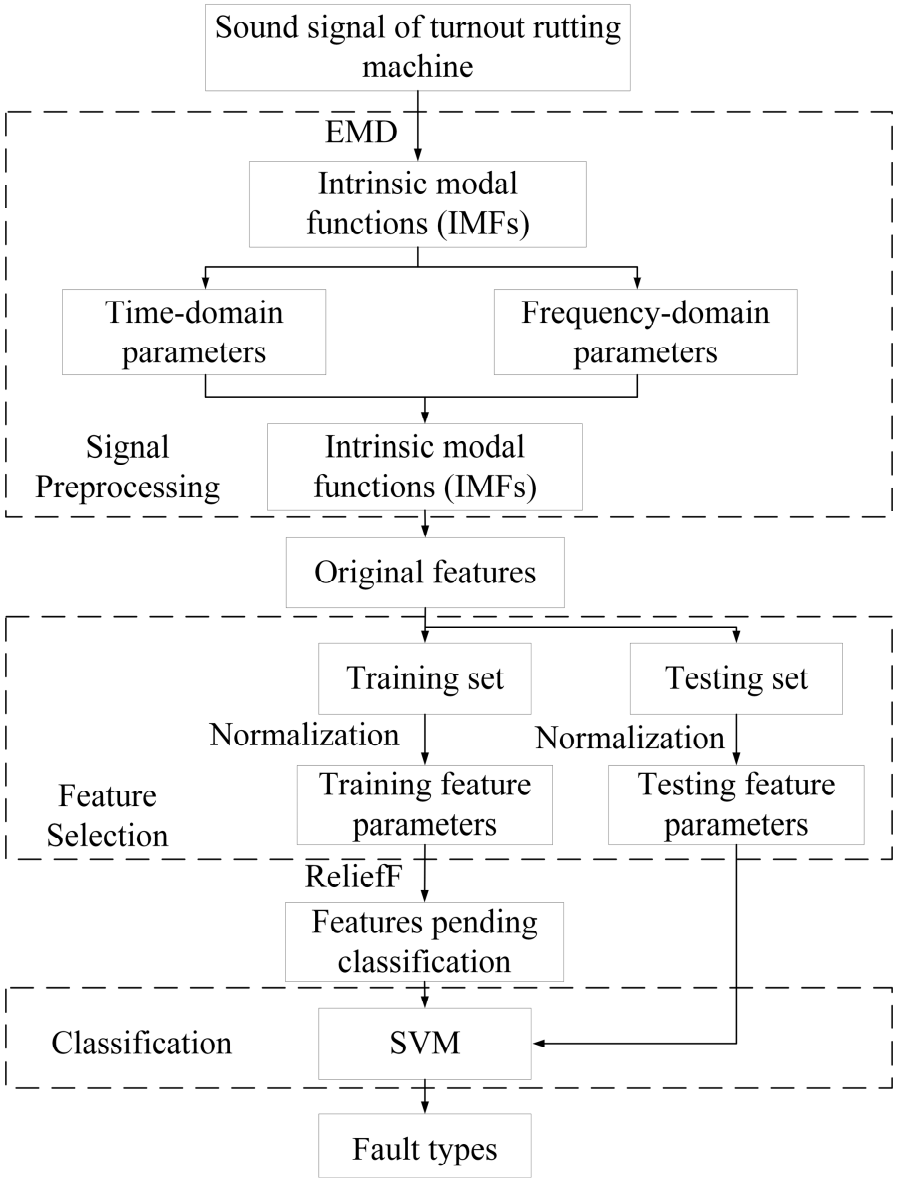


Figure 1. Execution process of ERS.

2.1. EMD Algorithm

EMD has been widely applied to the problems of denoising [18], feature extraction [19], and prediction [20]. Moreover, it has the ability to intelligently decompose the source signal into a set of intrinsic modal functions (IMFs) and a residual component, allowing for the extraction of detailed information from the non-stationary and nonlinear signals of mechanical equipment [21–24]. The pseudo-code of the EMD algorithm is shown in Algorithm 1.

Algorithm 1. The pseudo-code of the EMD algorithm

Input: the original signal, $x(t)$;
# Find local maxima and minima
maxima = find_local_maxima($x(t)$);
minima = find_local_minima($x(t)$);
# Fit upper and lower envelopes
$e_+(t)$ = fit_upper_envelope(maxima);
$e_-(t)$ = fit_lower_envelope(minima);
Compute the mean of the envelopes
$m(t) = (e_+(t) + e_-(t))/2$;
Calculate the residual
$r_n(t) = x(t) - m(t)$;
# Check if the residual satisfies two IMF conditions
if satisfy_IMF_conditions($r_n(t)$) **then**
    $n = n + 1$;
    $c_n(t) = r_n(t)$;
    $x(t) = x(t) - c_n(t)$;
else
    goto step 1;
end if
# Check if the residual is a monotonic function or constant
if is_monotonic_or_constant() **then**
    break;
else
    goto step 1;

In Algorithm 1, two IMF conditions are as follows: (1) The number of extrema must equal the number of zero crossings, or their difference must not exceed one. (2) At any moment, the mean of the upper and lower envelopes, determined by the local peaks and troughs, should equal zero. In addition, $m(t)$, $r(t)$, and $c_n(t)$ are the mean envelope, the intermediate variable, and the nth IMF, respectively. The decomposed signal of the original signal can be described as follows:

$$x(t) = \sum_{1}^{n} c_n(t) + Res \tag{1}$$

In Equation (1), $x(t)$ and Res represent the original signal and the residuals, respectively.

2.2. ReliefF Algorithm

When dealing with high-dimensional data, there are inevitably a large number of redundant and irrelevant features. It not only increases the complexity and time consumption of data processing but also reduces the accuracy of data classification to some extent. As a filter method with relatively low computational complexity and relatively higher speed, the ReliefF algorithm is an extension of Relief for the binary classification problem based on a distance criterion or correlation [25,26].

Against multi-classification problems, the RelifF algorithm randomly selects a sample R from the training set and then finds k nearest neighbor samples (near Hits) of R from the sample set of the same class as R, denoted as H_j. Also, it finds k nearest neighbor samples from the sample sets (near Misses) of each different class from R, denoted as $M(C)_j$, and

then updates the weight of each feature. For example, the feature weight $W(A)$ of feature A in the sample set is as shown in Equation (2) below [25,26]:

$$W(A) = W(A) - \frac{\sum_{j=1}^{k} d\left(A, R, H_j\right) + \sum_{C \neq class(R)} \frac{P(C)}{[1-P(class(R))]} \cdot \sum_{j=1}^{k} d\left(A, R, M(C)_j\right)}{(m \cdot k)} \quad (2)$$

In the equation, $Class(R)$ is the class of the randomly selected sample; $P(C)$ is the probability of class C occurring; $P(class(R))$ is the probability of $Class(R)$; $d(A,\ R,\ H_j)$ and $d\left(A, R, M(C)_j\right)$ are the distances between both H_j and $M(C)_j$ to feature A, respectively; and m is the number of sampling times. ReliefF can provide weights for different features. The features with a larger weight possess higher discriminatory power. Therefore, ReliefF is used to reduce the dimensionality of the original feature set.

2.3. SVM Algorithm

For classification problems, SVM is a class of generalized linear classifiers that classify binary data in a supervised learning fashion. SVMs are known for their ability to generalize well to unseen data, which is crucial in fault diagnosis where the model must accurately predict faults even with new, previously unencountered, conditions [27,28]. The decision boundary is a maximum margin hyperplane solved for the learning samples. It enables the conversion of the issue into a solution for convex quadratic programming. The computation for solving the problem is the inner product (or dot product) when transformed into an optimization problem in linear SVM. Then, the vector points in the training set $\phi(X)$ are converted into a nonlinear and high-dimensional mapping function. Given that the algorithmic complexity of the inner product is greater, the kernel function is used to compute the inner product of the nonlinear mapping function. The problems of dimensional catastrophe and nonlinear differentiability can be overcome. Due to the high dimensionality of the data in this experiment and the nonlinear nature of the problem, the radial basis function (RBF) was used as the SVM kernel, as is shown in Equation (3):

$$K(x, x_i) = exp\left(-\|x - x_i\|^2 / 2\sigma^2\right) \quad (3)$$

In (3), x and x_i are two sample points in the input space; σ is a hyperparameter; and $exp(\cdot)$ is the Gaussian function. In addition, the SVM classification decision function is shown in Equation (4) below:

$$f(x) = sign\left(W^T x + b\right) \quad (4)$$

In Equation (4), $sign(\cdot)$ is the sign function; $f(x)$ equals 1 if $f(x)$ is of positive class and -1 if $f(x)$ is of negative class.

3. Experiment Results

To verify the effectiveness of EMD-RelifF-SVM, the collected sound signal for fault diagnosis was processed by the proposed method. In addition, the comparison of classification results obtained from training SVM using all features (without feature selection) and features after dimensionality reduction by the RelifF algorithm was conducted and analyzed. The experimental setting was based on our previous publication [29].

3.1. Sound Signal Acquisition

The sound signal was recorded from the ZDJ9 switch machine, as shown in Figure 2, under 10 different working conditions using a portable recorder (PCM-D50) with a sampling frequency of 44.1 kHz for the more clear IMFs [30]. According to the onsite investigation, 10 states of ZDJ9 in both the positioning and reversing work were collected from Xi'an Railway Signal Co., Ltd., Xi'an, China (refer to the website: http://xaxh.crsc.cn/g4243.aspx (accessed on 28 November 2024)), as shown in Table 1. Each state contained 80 samples of

the sound data, totaling 1600 samples. Each sample was collected for 7 s; thus, there were approximately 308,700 sampling points.

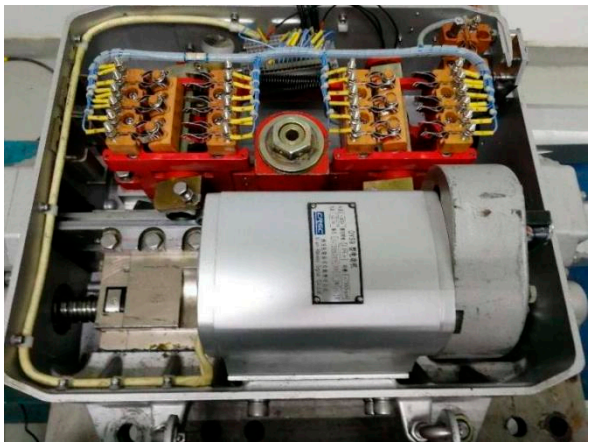


Figure 2. Internal view of the turnout switch machine.

Table 1. Ten work states of the ZDJ9.

Type	States Description	Type	States Description
A	No load	F	Loose gearbox bite
B	Normal	G	Gearbox knocking sound, Level I
C	Signposts not in place	H	Gearbox knocking sound, Level II
D	Friction	I	Gearbox overbite, Level I
E	Jamming	J	Gearbox overbite, Level II

Figure 3 presents the time domain waveforms for 10 states in the positioning work. As depicted in Figure 3, the switching process takes more time under normal load conditions (Type B) compared to no load (Type A). Type B shares similarities with Type C, except for the presence of an impact sound between the moving and fixed contacts within the switch circuit controller, which is characteristic of Type B. An increase in friction between the slide plate and the turnout belt correlates with a longer switching time (Type D), and the motor generates higher torque, resulting in distinct sound signals. In Type E scenarios, despite motor operation, the throw bar remains immobile due to obstructions, leading to an absence of locking sounds and an extended switching duration beyond the standard 5.8 s. Failures in the retarder, progressing from Type F to Type J, exacerbate damage, which is evident in the unusual sound emissions. Loose gear meshing in the retarder results in metallic impact noises, while tight meshing produces a high-pitched sound. Pitting of gear teeth leads to knocking sounds, with the intensity of the abnormal sound increasing in line with the severity of the damage (for example, Type H and Type J).

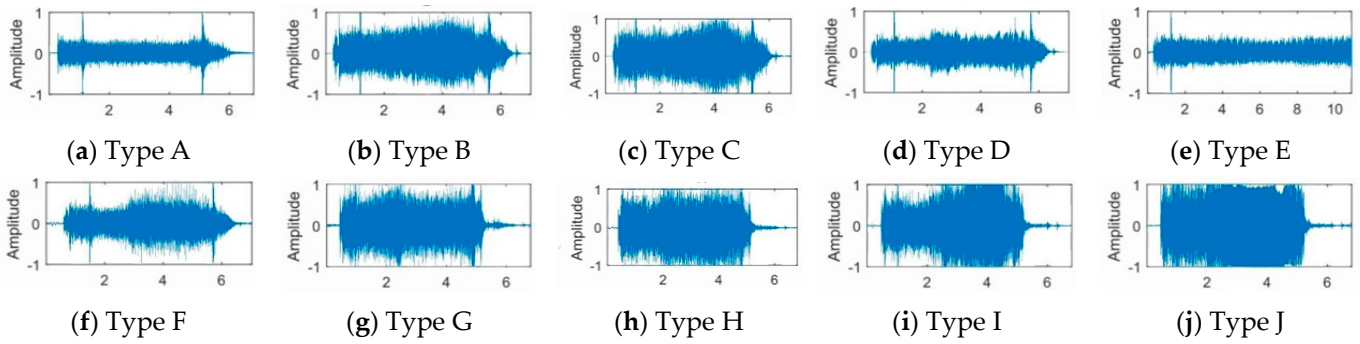


Figure 3. Ten types of time domain waveforms in the positioning work. Note that the x-coordinate of all figures denotes the time (s).

3.2. Training Set and Testing Set

Considering that the data samples (sound signal) needed for classifier training and testing were different, and the normalization of data in the training set and testing set should be carried out separately without affecting each other, all data samples of sound signal were divided into the training set and the testing set. To maintain the consistency of variables, the number of samples for each working state in the training set or the testing set should be the same. Therefore, 80 data samples in each state were set up as 50 samples in the training set and 30 samples in the testing set to ensure classification accuracy.

Due to the large disparity among the extracted feature data, the magnitude of the extraction values for different features of the same sample ranges from 10^{-3} to 10^{5}. This results in the lower-order magnitude values being easily overshadowed in the subsequent feature selection and classification processes, leading to increased errors, inaccurate classification, and inconsistent feature dimensions, which prevents further data processing. According to Section 3.1, the sound signal can reflect abnormalities in rotational speed, as is shown in Figure 3. Nevertheless, the sound signal of rotational speed, being a form of vibration signal, typically exhibits non-stationary and nonlinear characteristics. For in-depth analysis, EMD was employed to preprocess the signals into a stationary form. As an illustration, Figure 4 displays the initial 16 IMFs derived from Type A.

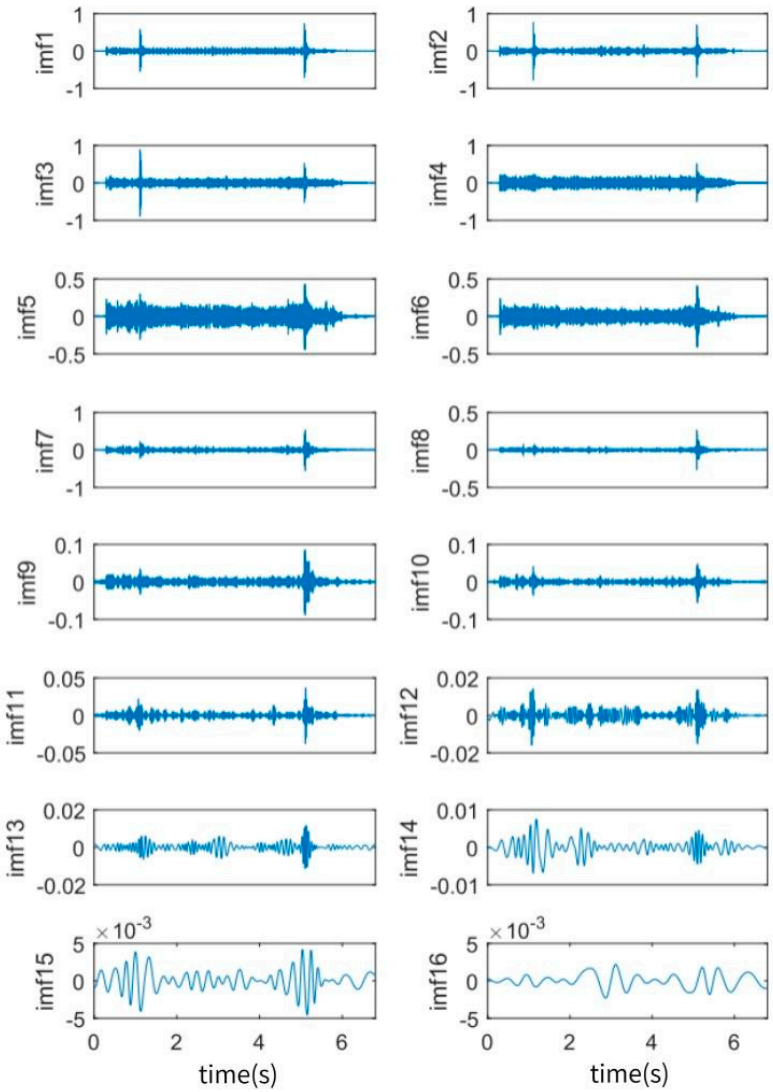


Figure 4. The first 16 IMFs of Type A sound signals.

It can be seen from Figure 4 that the initial few IMFs contain high-frequency information, which can reflect most of the information from the original signal. The last few IMFs, on the other hand, include low-frequency information and have small amplitudes. For quantitative analysis, this paper considered the first 15 IMFs for further examination. Subsequently, for each IMF, 10 time domain statistic features (mean, standard deviation, kurtosis, skewness, RMS, RMS amplitude, margin factor, shape factor, crest factor, pulse factor) and 3 frequency domain features (center of gravity frequency, RMS frequency, frequency standard deviation) were extracted. Thus, the dimension of extracted features was 15 × 13 = 195. Then, normalization is necessary to eliminate the effect of different dimensions. The normalization formula is shown in Equation (5) below:

$$\overline{x} = \frac{x - Mean(x)}{var(x)} \tag{5}$$

where x, $Mean(x)$, and $var(x)$ denote the vector features, mean, and variance required for normalization, respectively. In addition, kurtosis, skewness, and RMS can be used for quantitative assessment of EMD's noise reduction effect [31].

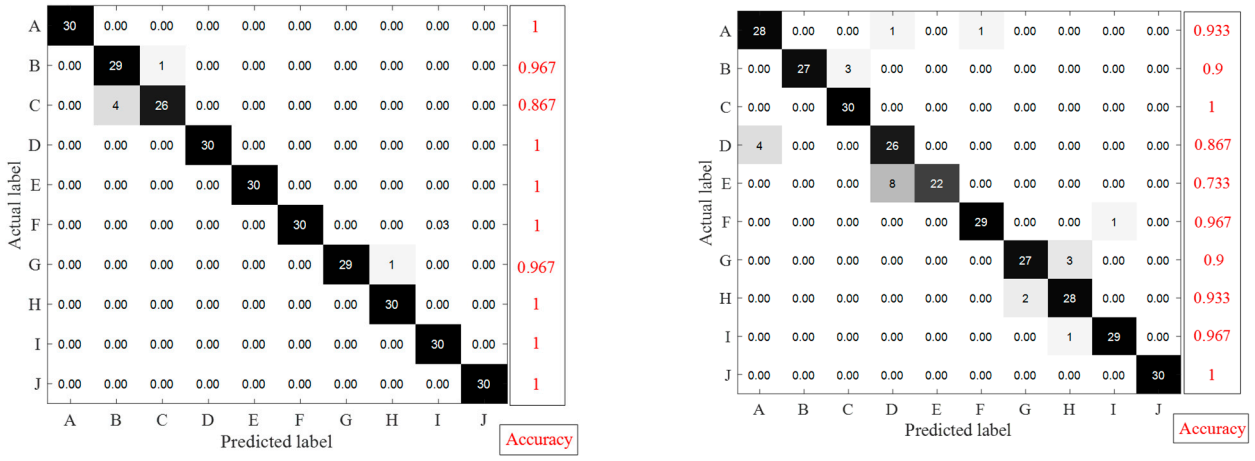
3.3. Results and Discussion

After the dataset was obtained, SVM classification was performed. For the SVM classification model, the two hyperparameters that needed to be tuned were the penalty coefficient C and the coefficient γ of the RBF kernel function. In principle, C should be as large as possible, and γ should be as small as possible. Through continuous enumeration and testing to achieve the most ideal parameter settings, the final parameter settings obtained in this experiment are as follows: for the positioning work mode, C was set to 1000 and γ was set to 0.01; for the reversing work mode, C was set to 1000 and γ was set to 0.02. The following is a discussion of the classification results with and without the ReliefF algorithm for feature selection.

The features without the ReliefF algorithm for feature selection were used to train the classifier (SVM). It was validated and tested using the testing set. When the testing set is used for testing, the classification accuracy of the positioning work mode can reach 98% at 95 iterations. However, the classification accuracy of the reversing work mode was only 92% at 121 iterations. Furthermore, the number of total support vectors was 210 and 203, respectively. The accuracy rate of the test results for each working state in the positioning mode and the reversing mode can be shown in Figure 5. Figure 5 is the confusion matrix demonstrating the tested results and accuracy rate for each state. It is noted that the horizontal table header is for the predicted labels, and the vertical table header is for the actual labels. The numbers in the confusion matrix of Figure 5 represent the number of tests for the corresponding predicted labels. The figures following Figure 5 adhere to the same format. It can be found from Figure 5 that, during the positioning work mode, the classification accuracy of the other working states reaches above 0.96, except for the C-type state with a lower classification accuracy of only 0.867. Moreover, during the reversing work mode, the classification accuracy of the E-type state is only 0.733, and that of the D-type state is also lower at only 0.867. The working states with a classification accuracy of 0.967 are of only four types. Therefore, although the classification accuracy of all features is high in the positioning work mode, the classification accuracy of all features in the reversing work mode is not satisfactory.

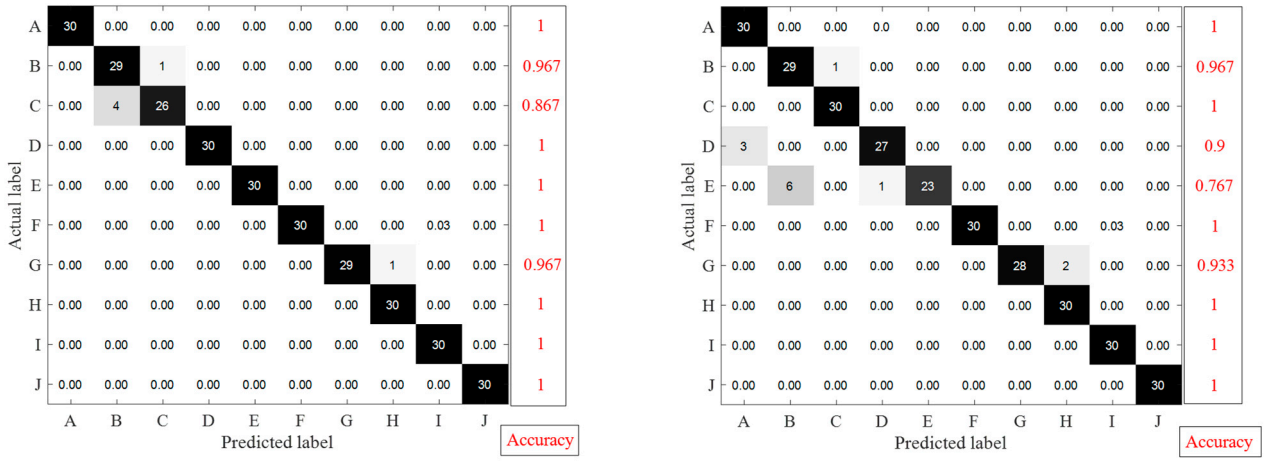
After the features with the ReliefF algorithm for feature selection (feature points whose weight larger than 0 is reserved) are used to train the classifier (SVM), the classification accuracy of positioning work mode can reach 98% at 64 iterations. However, the classification accuracy of reversing work mode is only 95.6667% at 71 iterations. Furthermore, the number of total support vectors is 222 and 229, respectively. The confusion matrices and accuracy rates of the dimensionality reduction feature testing in both positioning and reversing work modes are shown in Figure 6. Also, it can be seen from the figure that, during the positioning work mode, the classification accuracy of the other working states

reaches above 0.96, except for the C-type state with a lower classification accuracy of only 0.867. This is the same as that of the full-feature test results. Moreover, during the reversing work mode, the classification accuracy of the E-type state is lower by only 0.767, but that of the D-type state is improved to reach over 0.9 concerning the full-feature training. The working states with a classification accuracy of 0.967 are of seven types. The accuracy of classification of almost all types of action states improved. Therefore, for the positioning work mode, there was no difference in testing results between the trained features with and without the ReliefF algorithm, but the classification accuracy of dimensionality reduction features increased significantly under the reversing work mode.



(**a**) (**b**)

Figure 5. Confusion matrix (CM) for full-feature testing. Noted: Red numbers denote the accuracy, and the depth of color in the picture indicates the magnitude of the value. (**a**) Positioning work mode; (**b**) reversing work mode.



(**a**) (**b**)

Figure 6. Confusion matrix (CM) for dimensionality reduction feature testing. Noted: Red numbers denote the accuracy, and the depth of color in the picture indicates the magnitude of the value. (**a**) Positioning work mode; (**b**) reversing work mode.

Furthermore, comparing the iterations of the full features, the iteration count for the feature's dimensionality reduction was markedly decreased. The iteration in the positioning work mode reduced from 95 to 64, and that in the reversing work mode reduced from 121 to 71. This indicates that the feature dimensionality reduction effectively improves the algorithm computing speed and classification efficiency. In addition, the number of

total support vectors improved from 210 to 222 in the positioning work mode, and from 203 to 229 in the reversing work mode. Also, it can be demonstrated from Table 2 that the performance metrics of the confusion matrix for the reverse mode all improved after using feature selection, even though those for the positioning work mode remained unchanged. This indicates that the classification hyperplane formed by SVM training is more and more accurate, and can better identify the support vectors and classify them accurately after feature selection of the ReliefF algorithm. In summary, the efficiency and accuracy of the classifier can be significantly improved by the dimensionality reduction in the data through feature extraction.

Table 2. The performance metrics of two confusion matrices.

Performance Metrics		Positioning Work Mode	Reversing Work Mode
Full feature	Precision	0.98	0.92
	Recall	0.98	0.92
	F1-score	0.98	0.92
Feature selection	Precision	0.98	0.9567
	Recall	0.98	0.9567
	F1-score	0.98	0.9567

4. Conclusions

The existing methods are not conducive to collecting a large amount of data, and they are also susceptible to interference from human factors. In this study, considering the advantages of easy collection and contactlessness of sound signals, a sound-signal-based fault diagnosis method for railway turnout switch machines named ERS was proposed. According to the experiment results and comparisons, it can be concluded that EMD is an efficient mean for preprocessing nonlinear and non-stationary sound signals. In addition, ReliefF is significantly beneficial for removing redundant features and improving the diagnosis accuracy. Though the diagnosis effects are good on both positioning and reversing work modes, their diagnosis accuracies differ a little, which is caused by the asymmetric structure of switch machines. Overall, the ERS method achieved better performance, holding significant potential for fault diagnosis in railway turnout switch machines. However, some samples of Type E are easily identified as the other kinds of faults due to the similarity of their features.

In the future, we will conduct studies to further improve the diagnosis accuracy of each kind of fault. We plan to explore more advanced feature extraction techniques to better discriminate between similar fault types. In addition, we will focus on addressing the practical challenges of deploying our fault diagnosis method in real-world environments, including optimizing sensor placement, enhancing noise resilience, and ensuring system robustness against variations in sound source location and fault types, to facilitate broader industrial applications.

Author Contributions: Methodology, X.T. and Y.S.; validation, X.T.; writing—original draft preparation, Y.L. and X.T.; writing—review and editing, Y.L.; funding acquisition, Y.L. All authors have read and agreed to the published version of the manuscript.

Funding: This work was supported by the National Natural Science Foundation of China (Grant No. 62301159) and the Natural Science Foundation of Fujian Province (Grant No. 2023J01229).

Data Availability Statement: Data are contained within the article.

Conflicts of Interest: The authors declare no conflicts of interest.

References

1. Gao, Y.; Yang, Y.; Ma, Y.; Xu, W. Study on intelligent diagnosis of railway turnout switch based on improved FastDTW and time series segmentation under big data monitoring. *Math. Probl. Eng.* **2022**, *2022*, 7048813. [CrossRef]
2. Ji, W.; Zuo, Y.; Hei, X. An intelligent fault diagnosis model based on FastDTW for railway turnout. In Proceedings of the 13th EAI International Conference on Mobile Multimedia Communications, Cyberspace, 27–28 August 2020.
3. Reetz, S.; Neumann, T.; Schrijver, G.; van den Berg, A.; Buursma, D. Expert system based fault diagnosis for railway point machines. *Proc. Inst. Mech. Eng. Part F J. Rail Rapid Transit* **2024**, *238*, 214–224. [CrossRef]
4. Sun, Y.; Cao, Y.; Li, P.; Xie, G.; Wen, T.; Su, S. Vibration-based fault diagnosis for railway point machines using VMD and multiscale fluctuation-based dispersion entropy. *Chin. J. Electron.* **2024**, *33*, 803–813. [CrossRef]
5. Sun, Y.; Cao, Y.; Liu, H.; Yang, W.; Su, S. Condition monitoring and fault diagnosis strategy of railway point machines using vibration signals. *Transp. Saf. Environ.* **2023**, *5*, tdac048. [CrossRef]
6. Chen, H.; Jiang, B.; Ding, S.X.; Huang, B. Data-driven fault diagnosis for traction systems in high-speed trains: A survey, challenges, and perspectives. *IEEE Trans. Intell. Transp. Syst.* **2020**, *23*, 1700–1716. [CrossRef]
7. Lao, Z.; He, D.; Wei, Z.; Shang, H.; Jin, Z.; Miao, J.; Ren, C. Intelligent fault diagnosis for rail transit switch machine based on adaptive feature selection and improved LightGBM. *Eng. Fail. Anal.* **2023**, *148*, 107219. [CrossRef]
8. Wang, Z.; Wang, N.; Zhang, H.; Jia, L.; Qin, Y.; Zuo, Y.; Zhang, Y.; Dong, H. Segmentalized mRMR features and cost-sensitive ELM with fixed inputs for fault diagnosis of high-speed railway turnouts. *IEEE Trans. Intell. Transp. Syst.* **2023**, *24*, 4975–4987. [CrossRef]
9. Abbasnejad, S.; Mirabadi, A. Predicting the failure of railway point machines by using Autoregressive Integrated Moving Average and Autoregressive-Kalman methods. *Proc. Inst. Mech. Eng. Part F J. Rail Rapid Transit* **2018**, *232*, 1790–1799. [CrossRef]
10. Shi, Z.; Liu, Z.; Lee, J. An auto-associative residual based approach for railway point system fault detection and diagnosis. *Measurement* **2018**, *119*, 246–258. [CrossRef]
11. Lee, J.; Choi, H.; Park, D.; Chung, Y.; Kim, H.-Y.; Yoon, S. Fault detection and diagnosis of railway point machines by sound analysis. *Sensors* **2016**, *16*, 549. [CrossRef]
12. Gao, J.; Tembine, H. Distributed mean-field-type filters for big data assimilation. In Proceedings of the 2016 IEEE 18th International Conference on High Performance Computing and Communications; IEEE 14th International Conference on Smart City; IEEE 2nd International Conference on Data Science and Systems (HPCC/SmartCity/DSS), Sydney, Australia, 12–14 December 2016.
13. Hamadache, M.; Dutta, S.; Olaby, O.; Ambur, R.; Stewart, E.; Dixon, R. On the fault detection and diagnosis of railway switch and crossing systems: An overview. *Appl. Sci.* **2019**, *9*, 5129. [CrossRef]
14. Li, Z.; Yin, Z.; Tang, T.; Gao, C. Fault diagnosis of railway point machines using the locally connected autoencoder. *Appl. Sci.* **2019**, *9*, 5139. [CrossRef]
15. Chen, H.; Jiang, B. A Review of Fault Detection and Diagnosis for the Traction System in High-Speed Trains. *IEEE Trans. Intell. Transp. Syst.* **2020**, *21*, 450–465. [CrossRef]
16. Wang, Z.; Xiao, F. An improved multisensor data fusion method and its application in fault diagnosis. *IEEE Access* **2018**, *7*, 3928–3937. [CrossRef]
17. Sun, Y.; Cao, Y.; Li, P.; Su, S. Entropy feature fusion-based diagnosis for railway point machines using vibration signals based on kernel principal component analysis and support vector machine. *IEEE Intell. Transp. Syst. Mag.* **2023**, *15*, 96–108. [CrossRef]
18. Chen, X.; Xu, X.; Liu, A.; McKeown, M.J.; Wang, Z.J. The use of multivariate EMD and CCA for denoising muscle artifacts from few-channel EEG recordings. *IEEE Trans. Instrum. Meas.* **2017**, *67*, 359–370. [CrossRef]
19. Mohanty, S.; Gupta, K.K.; Raju, K.S. Hurst based vibro-acoustic feature extraction of bearing using EMD and VMD. *Measurement* **2018**, *117*, 200–220. [CrossRef]
20. Cao, Y.; Lu, H.; Wen, T. A Safety Computer System Based on Multi-Sensor Data Processing. *Sensors* **2019**, *19*, 818. [CrossRef]
21. Huang, N.E.; Shen, Z.; Long, S.R.; Wu, M.C.; Shih, H.H.; Zheng, Q.; Yen, N.-C.; Tung, C.C.; Liu, H.H. The empirical mode decomposition and the Hilbert spectrum for nonlinear and non-stationary time series analysis. *Proc. R. Soc. London. Ser. A Math. Phys. Eng. Sci.* **1998**, *454*, 903–995. [CrossRef]
22. Wu, H.; Yuan, R.; Lv, Y.; Stein, D.L.; Zhu, W. Multi-Weighted Symbolic Sequence Entropy: A Novel Approach to Fault Diagnosis and Degradation Monitoring of Rotary Machinery. *Meas. Sci. Technol.* **2024**, *35*, 106119. [CrossRef]
23. Wang, W.; Liu, W.; Lin, C.; Li, M.; Zheng, Y.; Liu, D. Fault detection system of subway sliding plug door based on adaptive EMD method. *Meas. Sci. Technol.* **2024**, *35*, 015102. [CrossRef]
24. Wang, W.; Jiang, Q.; Heng, X.; Liu, D.; Li, Z.; Xie, L. Fault Diagnosis of Subway Plug Door based on EEMD and Adaptive Feature Extraction. In Proceedings of the IEEE Conference on Industrial Electronics and Applications 2021, Chengdu, China, 1–4 August 2021.
25. Reyes, O.; Morell, C.; Ventura, S. Scalable extensions of the ReliefF algorithm for weighting and selecting features on the multi-label learning context. *Neurocomputing* **2015**, *161*, 168–182. [CrossRef]
26. Shi, S.; Li, G.; Chen, H.; Liu, J.; Hu, Y.; Xing, L.; Hu, W. Refrigerant charge fault diagnosis in the VRF system using Bayesian artificial neural network combined with ReliefF filter. *Appl. Therm. Eng.* **2017**, *112*, 698–706. [CrossRef]
27. Chen, J.; Wang, J.; Zhu, J.; Lee, T.H.; de Silva, C.W. Unsupervised cross-domain fault diagnosis using feature representation alignment networks for rotating machinery. *IEEE/ASME Trans. Mechatron.* **2020**, *26*, 2770–2781. [CrossRef]

28. Zhang, J.; Song, X.; Gao, L.; Shen, W.; Chen, J. L2-norm shapelet dictionary learning-based bearing-fault diagnosis in uncertain working conditions. *IEEE Sens. J.* **2021**, *22*, 2647–2657. [CrossRef]
29. Cao, Y.; Sun, Y.; Xie, G.; Li, P. A Sound-Based Fault Diagnosis Method for Railway Point Machines Based on Two-Stage Feature Selection Strategy and Ensemble Classifier. *IEEE Trans. Intell. Transp. Syst.* **2021**, *23*, 12074–12083. [CrossRef]
30. Govind, V.; Rajesh, K. An effective health indicator for the Pelton wheel using a Levy flight mutated genetic algorithm. *Meas. Sci. Technol.* **2021**, *32*, 094003.
31. Govind, V.; Rajesh, K. Autocorrelation energy and aquila optimizer for MED filtering of sound signal to detect bearing defect in Francis turbine. *Meas. Sci. Technol.* **2022**, *33*, 015006.

Disclaimer/Publisher's Note: The statements, opinions and data contained in all publications are solely those of the individual author(s) and contributor(s) and not of MDPI and/or the editor(s). MDPI and/or the editor(s) disclaim responsibility for any injury to people or property resulting from any ideas, methods, instructions or products referred to in the content.